Astrometric planet detectability with Gaia, a short AGISLab study

prepared by: B. Holl
affiliation : Lund Observatory
approved by:
reference: GAIA-C3-TN-LU-BH-003-01
issue: 1
revision: 0
date: 2011-09-15
status: Issued

Abstract

This note describes the results of a planet-course project in which the Gaia detectability of a planet in circular orbit around a solar-like star was studies with AGISLab. Besides a short theoretical background we describe how we modelled and simulated our data. For the solar-type star our results show that planets are detectable when their period is between 4 months and 10 yr (outer bounds), peaking in sensitivity around 5 yr (the mission length). A $3M_{jup}$ planet could be detectable up to 300pc under the right conditions. The lowest mass we found detectable was $33M_{earth}$ (=$0.3M_{Sat}$). Lighter planets were undetectable because the minimum distance limit was 16pc (the distance at which a solar-like star has the maximum observable brightness of mag 5.7).

Contents

1 Introduction

This note describes the results of a project I proposed to do as part of the Planet Formation course in Lund. *The goal of this project is to study the detectability of a single planet around a solar-like star with Gaia.* Some underlying questions that I set for this project were:

- **How do we model an astrometric planet signal?**
  This is being addressed in different facets in Sect. 3, 4 and 5.
- **What is Gaia's astrometric detectability of a planet in circular orbit around a solar-type star?**
  This is about the results and therefore treated in the end in Sect. 7 and 8.
- **How to estimate the expected number of planet detected with Gaia?**
  The small Sect. 6 is dedicated to address this question.

As will become clear, the first two questions have been given the most attention. It should be noted that this project has been carried out in a limited amount of time (∼110 hours in 9 days for programming, analyzing, presenting and writing), and it is therefore by no means an extensive treatment of the topic. I just hope you will enjoy reading about this project as much as I enjoyed working on it!

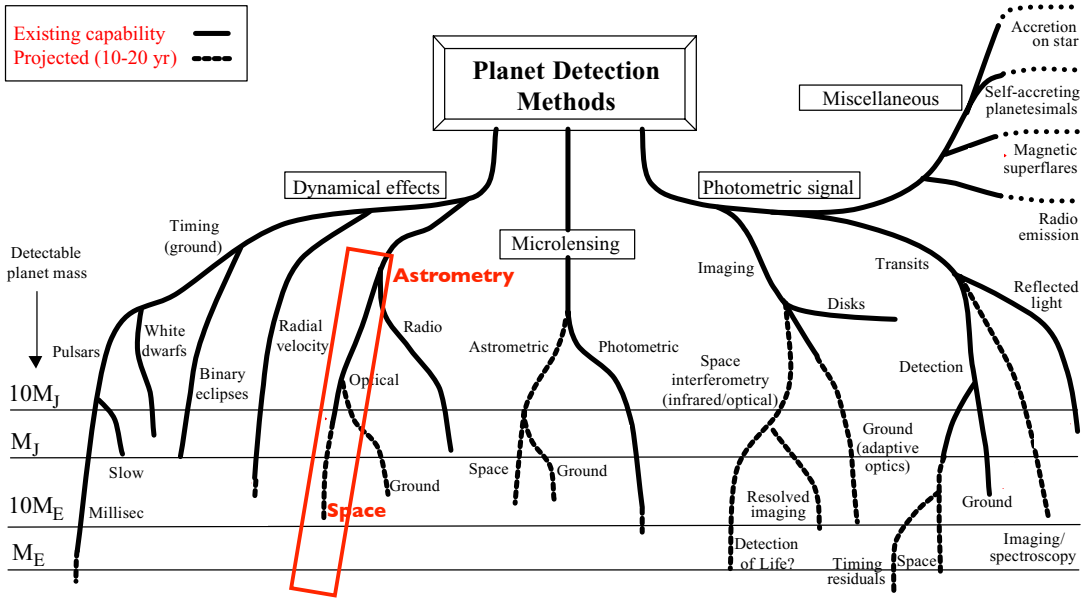

FIGURE 1: Overview of possible planet detection methods. In this project we focus on space astrometry, indicated in red. Image adapted from Perryman (2000).

2 Methods of planet detection

There are many ways to search for the presence of planets around other stars. A good overview of current and future methods is given in Perryman et al. (2005), a report from the ESA-ESO Working Group on Extra-Solar Planets. A graphical overview of these methods is given in Fig. 1. We will in this report focus on the astrometry method, especially from space using Gaia. A good review of astrometric methods and instrumentation of exo-planet detection can be found in Sozzetti (2005).

2.1 Astrometric detection method

For a single star, the 6-dimensional position and velocity components can be modelled using: position (α, δ), parallax (ϖ), proper motion (μ_α, μ_δ) and radial velocity (r). As astrometric observations only measure the tangential stellar position on the sky the radial velocity components is normally very weak. When measuring positions over many years It becomes apparent through an in/decrease of the size of the parallax ellipse and ac/deceleration of the proper motion. For most stars these effects are so small that even for Gaia it can only be detected for fast moving, nearby stars. Therefore we will ignore the radial velocity in the rest of this study.

Fig. 2 shows an example of how a star would move on the sky as observed from Earth (or a satellite in an earth-like orbit). The proper motion causes the star to move in a straight line on the sky. Because the coordinates are given in the equatorial system (i.e. the origin is moving with the Earth) there is an additional elliptical parallax motion (with a 1 year period) caused by our moving viewpoint. The flatness of this ellipse depends on height of the star above/below the *ecliptic plane*: a star in the ecliptic plane would be observed to move back and forth on a straight line, while a star at the ecliptic pole would have a perfect circular motion (when the proper motion is subtracted). The angular size of the semimajor axis of this ellipse is the parallax ϖ and it is a measure of the distance

$$\varpi \text{ [asec]} = 1/d \text{ [pc]} \tag{1}$$

So to astrometrically detect a planet one has to fit for the five stellar astrometric parameters α, δ, ϖ, μ_α and μ_δ, *plus* additional parameters that model the positional offset due to the planet. The construction of such a model for the planet signal is the topic of the next section.

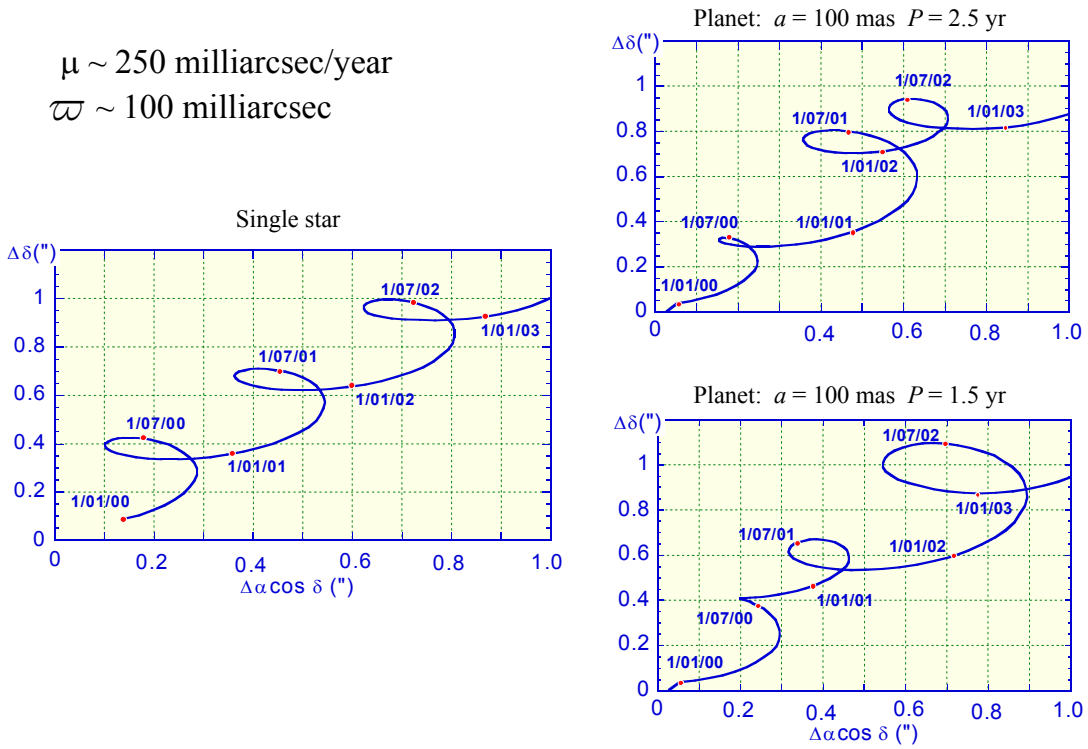

FIGURE 2: Examples of the apparent stellar motion of a star at 10 pc as observed from an observer moving in a circular orbit at 1AU. The left panel shows the apparent stellar motion for a single star over 3 years. The top right panelshows the same star with an exo-planet (probably with a face-on orbit) having a period of 2.5 year and an *astrometric signal* a (see Sect. 3.1) of 100 mas (as large as the parallax signal). In the bottom right panel the planet's period has been shortened to 1.5 year. Image adapted from M. Perryman (2004), presentation at 'Exploring the Cosmic Frontiers': *Detection and Characterization of Extra-Solar Planets*.

3 Modelling an astrometric planet signal

For the astrometric detection of planets we need to construct a model that parameterizes the orbital properties of the exoplanet system and predicts the time-dependent positional offset. For simplicity we model the position offsets of the star as angular offsets that are aligned with $\boldsymbol{p}$ and $\boldsymbol{q}$ (see Fig. 3). This means that we can simply add these $\Delta\alpha^*$ and $\Delta\delta$ offsets to the star position at time t (the asterisk in $\Delta\alpha^* \equiv \Delta\alpha\cos\delta(t)$ being the true arclength offset on the sky)

$$\begin{aligned} \alpha(t) &= \alpha_0 + \mu_\alpha(t-t_0) + \Delta\alpha^*(t)/\cos\delta(t) \\ \delta(t) &= \delta_0 + \mu_\delta(t-t_0) + \Delta\delta(t) \end{aligned} \tag{2}$$

Here the basic time dependent position of the star is expressed as the position of the star at its reference epoch t_0 (α_0, δ_0) plus proper motion (μ_α, μ_δ). Note that we did not include a radial velocity component. For Gaia these parameter are expressed in the International Coordinate Reference System (ICRS) which is very closely aligned with the equatorial reference system,

but has it's origin fixed at the barycentre (i.e. the mass centre) of our solar system instead of the centre of the earth. Therefore there is no parallax signal in Eq. (2), while it is included in Fig. 2 as that shows the star position in equatorial coordinates.

3.1 Astrometric signal

An important parameter in astrometric planet detection is the *astrometric signal* a: the maximum angular offset of a star with respect to the planet & star centre of mass, as observed from a distance d (Casertano et al., 2008)

$$a\ [\text{asec}] = m_{ratio} \times s_{planet}\ [\text{AU}]/\ d\ [\text{pc}] \qquad \text{with} \quad m_{ratio} = \frac{m_{planet}}{m_{star}} \tag{3}$$

Here s_{planet} is the semimajor axis of the planet. It can intuitively be understood why a follows this relation: increasing the mass ratio or semimajor axis will in both cases linearly move the centre of mass further away from the star, while the spanned angle of the separation (in small angle approximation) scales inversely with distance. Note that we can substitute distance by parallax using Eq. (1).

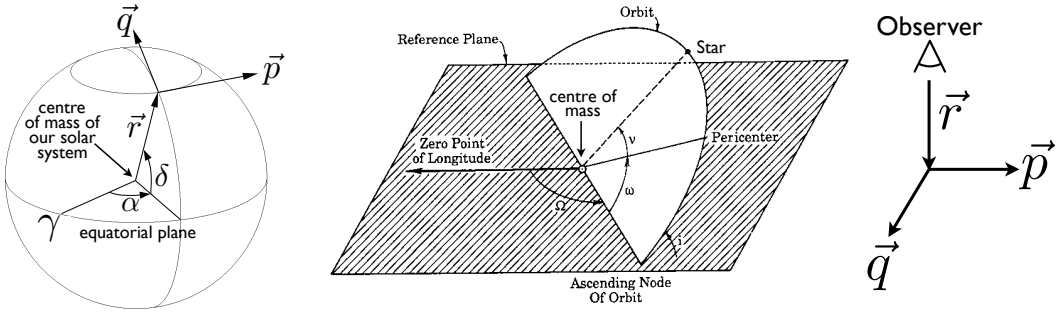

FIGURE 3: Geometry of the positional displacement of a star due to the presence of a planet. Left image shows the International Celestial Reference System (ICRS) with the star position in the sky expressed in ra and dec (α, δ). The *local triad* is formed by three unit vectors: $\boldsymbol{p}$ pointing towards increasing α, $\boldsymbol{q}$ pointing towards increasing δ, $\boldsymbol{r}$ pointing toward the positions on the sky. Image adapted from the 'Dynamical astronomy' syllabus, L. Lindegren (2010). Right image shows the geometry and parametrisation of the orbit of a star around the star & planet centre of mass. Parameters involved are: the astrometric signal a, e the eccentricity, ν the true anomaly (the angle between the planet's pericentre and its current position), i the inclination of the orbit, Ω the longitude of the ascending node, and ω the argument of the pericentre. Image adapted from Hamilton (1993).

3.2 Elliptical orbit

For modelling the astrometric signal in the star offsets we adapt the formulation as used in Casertano et al. (2008, Eq. (A.2) & (A.3)). We orient the angular position offsets of the star (see Fig. 3) such that they can be directly used to get the time-dependent position on the sky

$$\begin{aligned} \Delta\alpha^*_{ellipse}(t) &= a\,(1 - e\,\cos E(t))\,[\cos(\nu(t)+\omega)\,\cos\Omega - \sin(\nu(t)+\omega)\,\sin\Omega\,\cos i] \\ \Delta\delta_{ellipse}(t) &= a\,(1 - e\,\cos E(t))\,[\cos(\nu(t)+\omega)\,\sin\Omega - \sin(\nu(t)+\omega)\,\cos\Omega\,\cos i] \end{aligned} \quad (4)$$

with E the eccentric anomaly, which is the solution to Kepler's equation

$$E(t) - e\,\sin E(t) = 2\pi\frac{(t-t_0)}{P} \quad (5)$$

We will deviate from the formulation in Casertano et al. (2008) which treats t_0 as one of the free model parameters. We find it more convenient to set t_0 to the fixed reference epoch of the host star, which is typically set to a time halfway in the mission and is therefore unrelated to the planetary phase. As it is the orbital starting phase that we really want to parametrize we introduce the free parameter ϕ_0, which we will simply call the *start phase*. The true anomaly $\nu(t)$ (in simple words: the time dependent phase angle in the rotational plane measured from the pericentre angle ω) is therefore now not only a function of the eccentricity and eccentric anomaly, but also of the starting phase

$$\nu(t) = 2\,\arctan\left[\left(\frac{1+e}{1-e}\right)^{1/2}\tan\left(\frac{E(t)}{2}\right)\right] + \phi_0 \quad (6)$$

In total this elliptical model has 7 free parameters: $a, e, P, \phi_0, \omega, i$ and Ω (for a given reference epoch t_0). Note that ω, i and Ω can be considered *external orientation* parameters as they depend on the relative alignment of the system with respect to the observer.

3.3 Circular orbit

In the case of a circular orbit $e = 0$. As we need a reference point in the orbit from which we measure ν, we define $\omega = 0$. The model of the astrometric signal in the star offsets for a circular orbit simplifies now to

$$\begin{aligned} \Delta\alpha^*_{circle}(t) &= a\,[\cos\nu(t)\,\cos\Omega - \sin\nu(t)\,\sin\Omega\,\cos i] \\ \Delta\delta_{circle}(t) &= a\,[\cos\nu(t)\,\sin\Omega - \sin\nu(t)\,\cos\Omega\,\cos i] \end{aligned} \quad (7)$$

with the true anomaly

$$\nu(t) = 2\pi\frac{(t-t_0)}{P} + \phi_0 \quad (8)$$

This circular model has 5 free parameters: a, P, ϕ_0, i and Ω (for a given reference epoch t_0).

3.4 Additional parameters

There might be more parameters that seem relevant for this problem, but as it turns out, for a given stellar-type (and corresponding mass) all other parameters are determined as well.
First of all there is the relation between semimajor axis and period given by the Newtonian generalization of Keplers third law: for two bodies orbiting their mutual centre of mass we find (de Pater & Lissauer, 2010, Eq. (2.11))

$$P^2 = \frac{4\pi s_{planet}^3}{G(m_{star} + m_{planet})} \tag{9}$$

with P the orbital period. When $m_{ratio} = 0$ the relation reduces to $P_{yr}^2 = s_{planet,AU}^3$, which we obviously do not consider as it removes our astrometric signal, Eq. (3).
Next, for a given stellar-type there is a corresponding absolute magnitude (assuming a certain position in the HR-diagram, normally on the Main Sequence), which gives us a relation between the distance and apparent magnitude. As the apparent magnitude determines the relative flux that is received, the astrometric position measurement from a (normal photon collecting) detector will have a lower accuracy when the star is further away.

4 Simulating Gaia with AGISLab

In this study we make use of AGISLab, a versatile software tool that has been developed as part of my PhD which can simulate Gaia-like astrometric solutions (see BH-002 for a detailed description). We list here the relevant capabilities of AGISLab that are used in this study:

- Generation of any star distribution on the sky. A random distribution is used in this study. Each star has 5 stellar astrometric parameters (α, δ, ϖ, μ_α and μ_δ) and a reference epoch t_0. It can be extended to also include a multi-planet system with:
  – Circular orbits (5 parameters per planet, using the model of Sect. 3.3).
  – Elliptical orbits (7 parameters per planet, using the model of Sect. 3.2).

- Generation of noiseless Gaia observations for stars, including the planet perturbations. This uses a large amount of models for: satellite attitude, orbit, instrument layout, accuracy, etc. It is beyond the scope of this report to go in detail about all these models or discuss how the observations are exactly computed, see BH-002 for more details. We will shortly highlight the attitude model in Sect. 4.1. For this study we have used the models that represent our best knowledge of how we expect Gaia to observe. We used a nominal mission duration of 5 years.

- Adding noise to the observations on the fly. The observations are generated noiseless, but they will include an estimated standard error based on the source magnitude (this mapping is done by the accuracy model, which is shortly described in

Sect. 4.2). When processing the data we perturb each observation with Gaussian noise having the standard error that was stored with the observation. This allows us to re-use the (computational expensive) generated observations and apply different noise realizations or even mimic different magnitude stars by re-setting the standard errors in them. We have however not re-used any observations in this study.

- Fitting source models with the 5 stellar astrometric parameters to observations that include a planetary signal. We fit both sources that just have these 5 single source parameters, as well as sources that additionally have the planetary parameters that exactly match the signal in the observations (these planetary parameters are fixed and set beforehand). The difference between the goodness of fit between these two source models is used to determine the detectability of planet, see Sect. 5. We have not attempted to fit for the planetary parameters as well, because this is a very complicated business which unfortunately is beyond the scope of this project.

4.1 Attitude model

The most relevant information about the attitude model is summarized by Fig. 4 and 5: due to the way Gaia scans the sky, using the so called Nominal Scanning Law (NSL), each position is transited by a field of view on average 70 times over a 5 year mission. The exact number of field transits depends on the position on the sky, mainly being a function of the distance from the ecliptic plane.

4.2 Accuracy model and gating

Due to the satellite's spin, the images of the sources will enter the focal plane from the left and move over the various CCDs, see Fig. 6. In this study we are only concerned with observations made with the skymapper (SM1–2) and astrometric (AF1–9) CCDs, since only they are used for direct astrometric measurements. Each transit therefore produces 10 astrometric observations (1 SM and 9 AF), leading to an average of 700 astrometric observations per source over 5 years.

The observation of these 10 CCDs will have a different noise level, which is modelled with our accuracy model. The most accuracy observations (and therefore contributing most to the solution) are AF1–9. Fig. 7 shows the observation accuracy of AF 2–9 (AF1 is read out slightly different but has a very similar accuracy model). The SMs have quite a different accuracy model (no gating for example), but as they have very low accuracy they contribute little to the solution and therefore they are not so important in this discussion.

Note that for stars brighter than magnitude 12 there is a saw-pattern in the accuracy model. This is due to *gating*: a change of integration time of the CCD to avoid pixel saturation (it means in reality that charge is only accumulated over a smaller fraction of the CCD). The gating jumps are located at: mag_g = [11.95, 11.47, 11.10, 10.34, 9.59, 8.84].

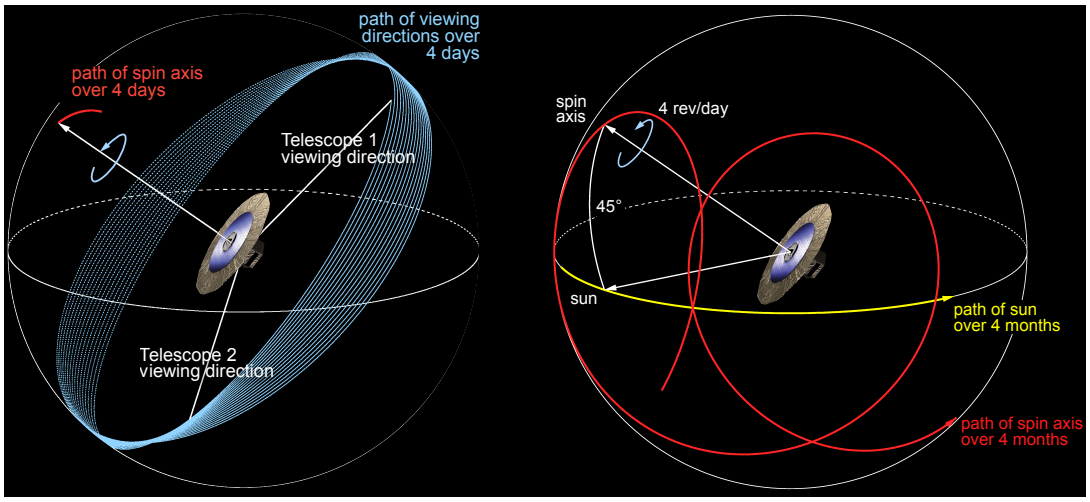

FIGURE 4: How Gaia scans the sky. Located near the second (L2) Lagrange point, 1.5 million km from the Earth, Gaia will be continuously spinning with a period of six hours. In the plane orthogonal to the spin axis it has two fields of view of $\sim$0.5 deg^2 that are separated by a basic angle of $106.5°$. The spin axis makes an angle of $45°$ to the solar direction, and precesses around this direction with a period of 63 days. This combination of spinning and precessional motions, known as the Nominal Scanning Law (NSL) of Gaia, ensures a reasonably uniform sky coverage over the mission lifetime of 5 years (see Fig. 5). Image credit: L. Lindegren.

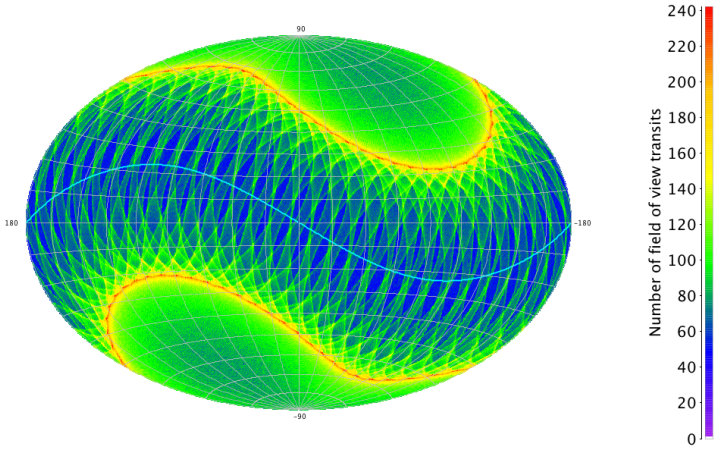

FIGURE 5: Colour-coded map of the expected number of field-of-view transits experienced by sources at different celestial positions after a 5 year mission. The projection uses ICRS ($\sim$equatorial) coordinates, with right ascension running from $-180°$ to $+180°$ right-to-left. The blue line is the ecliptic plane. The average number of field transits is 88 (or 72, accounting for downtime). An over-abundance of transits occurs at $45°$ away from the ecliptic plane due to the difference between the $45°$ spin axis angle with respect to the sun and the $90°$ angle between spin axis and the fields of view. Image generated with AGISLab.

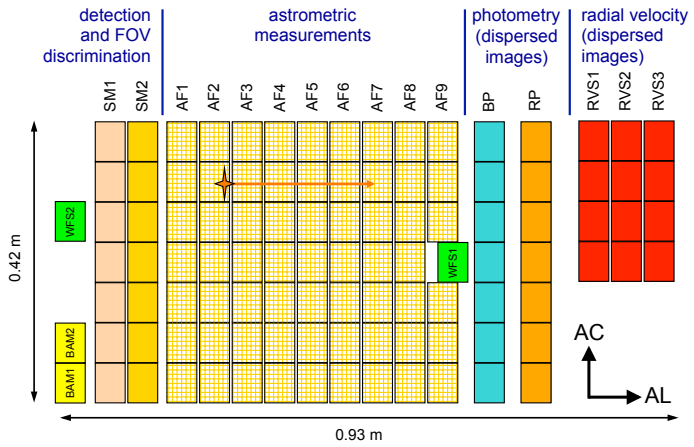

FIGURE 6: Schematic layout of the CCDs in the focal plane of Gaia. Due to the satellite spin, a source enters the focal plane from the left in along-scan (AL) direction. All sources brighter than 20 mag are detected by one of the sky mappers (SM1 or SM2, depending on the field of view) and then tracked over the subsequent CCDs dedicated to astrometry (AF1–9), photometry (BP and RP), and radial-velocity determination (RVS1–3). In addition there are special CCDs for interferometric basic-angle monitoring (BAM), and for the initial mirror alignment using wavefront sensors (WFS).

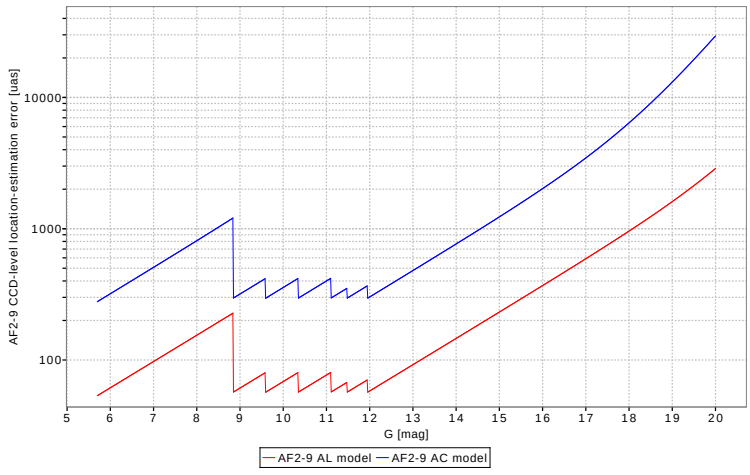

FIGURE 7: Accuracy model for Astrometric Field (AF) CCDs as function of G-magnitude. The saw-pattern up till 12th magnitude is due to gating in the CCDs (i.e. change of observation time to avoid pixel saturation).

Note that mag 5.70 is the brightest magnitude that can be observed with Gaia. Because the apparent magnitude of a particular star depends on the distance, the accuracy of the observations will be different as well. As it will turn out, the major accuracy jump for the gate at 8.84 appears to be visible in the planet detectability plots! (For example Fig. 10.)

5 Estimating Gaia planet detectability

We would like to start this section by pointing out the important difference between *planet detection* and *planet detectability* (Casertano et al., 1996). Planet *detection* is the determination of the mass and all orbital parameters of the planet(s). This means that each parameter has not only been fitted to a value but also has an associated (estimated) standard error that is within some reasonable limits. As we cannot fit orbital parameters with our current software, we are unable to assess planet detection with Gaia in this study.
In this study we can however study astrometric planet *detectability*, which in our case we defined as follows (see also Fig. 8):
Given that all source observations have the been generated with a planetary signal of a single planet in circular orbit, for which astrometric parameter combinations is there a significant difference in goodness of fit between:
(a) a fit of the 5 stellar parameters of a single star model, and
(b) a fit of the 5 stellar parameters of a star model that includes the planetary orbital parameters which exactly match the original signal used to generate the observations.
As we look at the difference between the worst model fit (not modelling the planet at all) and best model fit (all planetary parameters exactly correct) **our study gives a best-case detectability estimate**.

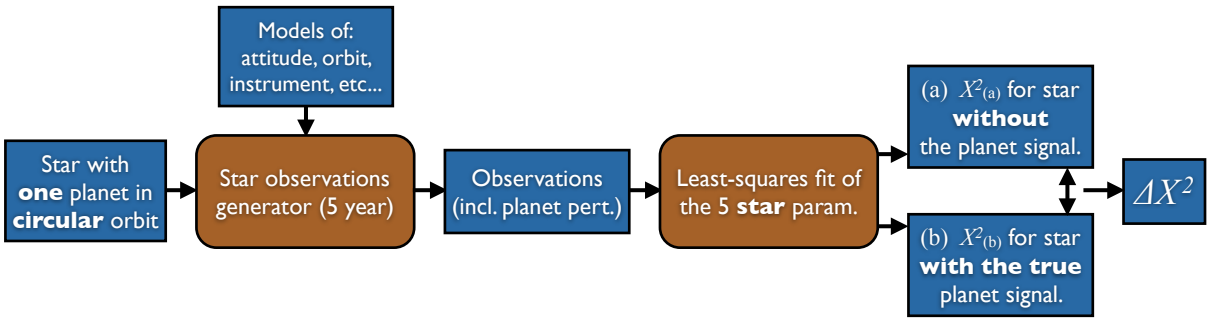

FIGURE 8: Main steps involved in computing goodness of fit that is used to test planet detectability.

5.1 Detectability and confidence criterion

As the noise in our observations is purely Gaussian, the least squares fit of the 5 stellar astrometric parameters will be equivalent to minimizing χ^2

$$\chi^2 = \sum_{i=1}^{k} \left(\frac{O_i - E_i}{\sigma_i} \right)^2 \tag{10}$$

with O_i an observed value, E_i the expected value from the model (based on the fitted parameters), σ_i the standard error associated with the observation, and k the number of observations.

We are not interested in the individual fit results of case (a) or (b) (although we have checked that the reduced χ^2 is close to 1), but we are interested in how significant the difference between the two values is: $\Delta\chi^2$. The answer can be found in e.g.Wall & Jenkins (2003, Sect. 6.4)

$$\text{if} \qquad \chi^2_{(a)} \geq \chi^2_{(b)} + \Delta(N,\alpha) \qquad \text{then planet detectability is significant at } \alpha \text{ level} \qquad (11)$$

with N the number of fitted parameters and α the significance level. Eq. (11) is now the criterion that tests our hypothesis: *a planet is detectable in the observations*. We will examine the detectability at the 0.05, 0.01 and 0.001 confidence levels, which are associated with $\Delta(5,\alpha)$= 11.07, 15.09 and 20.52 respectively (Wall & Jenkins, 2003, table A 2.6). This means for example that we have a confirmed planet detectability with a false-detection probability of $\leq$ 0.1% when $\Delta\chi^2 \geq 20.52$. It is interesting to note that $\Delta\chi^2$ does only depend on the number parameters involved and not on the goodness of fit itself (χ^2).

5.2 Estimating an orientation and sky averaged detectability

In our runs we will mainly try to estimate the detectability of a single planet on a circular orbit for many different *cases*. We define a *case* as a combinations of: orbital radius (s_{planet}), distance (d), significance level (α), mass ratio (m_{ratio}). As discussed in Sect. 3.4 we can substitute some of these parameters by others because they are coupled in certain ways.

Assuming that such an exo-planetary system will be randomly oriented with respect to the direction from which we observe the system (which seems perfectly legitimate), ϕ_0, i and Ω (see Sect. 3.3) will be uncorrelated between planetary systems of different stars. Therefore we would need to generate many different systems with random ϕ_0, i and Ω to get a good estimate of the detectability.

Another issue we have to address is best show by Fig. 5. Because the number of field of view transits varies largely as function of position on the sky, the detectability will also vary over the sky (as less observations with the same noise will make the difference between the goodness of fits smaller as well). Therefore we need to sample many positions over the sky to get a good estimate of detectability.

Because we would like to evaluate several hundred *cases* we want to keep the number of random orientations and sky positions, i.e. the number of *samples*, used for each *case* to a reasonable number. As we wrote our software to be fully multi-threaded and memory efficient we were able to run 1000 samples *per case* for roughly 1500 cases in only a few hours using 8 threads on a quad-core Xeon processor. Note that 1 sample means: generating a source with random orientations and position, generating 5 year of observations, making a least-squares solution of all observations to find the best fit of the 5 stellar astrometric parameters ($\times 2$ as we do it for both stellar models), and computing the χ^2 and $\Delta\chi^2$ of these best fits.

How to combine these 1000 samples per case?
Given our hypothesis which has only one outcome, *true* or *false*, we store for each sample that outcome. So the data stored for each case is an array containing 1000 samples with true or false. The only useful statistic that we can make out of this is: *what fraction of the sky (samples) has a positive detectability?* By colour coding different sky fractions in the final result plots we get an idea of the detectability for a certain case.

How to distribute these 1000 samples per case?
As we need to sample both the random orientation and sky distribution we distribute the 1000 stars randomly over the sky and give them each a random orientation. It could be that 1000 samples is not enough to give a 'stable' result, i.e. the sky fraction with positive detection would fluctuate too much for a given case. This has not been tested due to lack of time, but since we create a 'grid' of all the examined cases, the global trend would still be visible in the combined data plot. When we look for example at Fig. 10 in Sect. 7 it actually seems that 1000 samples does give a stable result because small 'features' seem to be consistent along different neighbouring cases.

6 Estimating expected number of planets

The way to compute the actual number of expected planets is nicely parametrized in SAG-AC-001:

$$n_p = \sum_i n_* P(D_i) P(p_i) \tag{12}$$

With the following elements:

- i sums over the discrete planetary and stellar characteristics (e.g. spectral type, stellar distance, period, planet mass).
- n_* is the number of stars in the Galaxy of certain spectral type at a specific distance. This can be retrieved from real sky catalogues or estimated using Galaxy models.
- $P(D_i)$ is the probability of detection of the specific (i) planet-star system. It also depends on all kinds of specific instrument properties like observation accuracy, number of observations, observations interval, etc. The work in this study is related to this part of the equation.
- $P(p_i)$ Probability of finding a planet of certain mass and period (mass distribution in space).

It seems that the latter three items are in order of how well they can be defined: the number density of stars has been mapped, catalogued and modelled very well. The detection probability

has been assessed in different papers, but as orbital parameter fitting is complicated, and the parameter space is large when fitting for example multiple planets, there seems still work to be done. And off course when Gaia is launched, fitting planetary parameters using the real data might behave differently than simulated... Last, and most uncertain of all seems to be the planet distribution in space, especially for the lower mass planets ($\lesssim 10 M_{earth}$, although Gaia might be not be able to detect those planets anyway).

7 Gaia planet detectability results

All the simulation that have been made are for a solar-type (G2V), solar-mass star with an absolute V-band mag 4.83. For each star there was one planet in circular motion around it.

7.1 Radius versus distance for solar-system-like planet masses

Our main result is the detectability exploration of the radius versus distance for the 6 mass ratios given below. In total 1545 cases were computed (=1,540,000 simulated source detectabilities, see Sect. 5.2 for more information). For all mass ratios the detectability was plotted for the 0.05, 0.01 and 0.001 confidence levels (meaning $\leq$ 5%, 1% and 0.1% false-detection of planet detectability). The data is summarized in Fig. 11, 12, and 13 at the end of this report. Fig. 9 illustrates the relative size of the astrometric signal.
An important boundary for planet detection around this solar-type star is the lower distance limit of 16pc. It is set by the accuracy model because Gaia cannot make observations of stars brighter than G-band mag 5.7, which corresponds to a minimum distance of 16pc for this stellar type.

Mass ratios and planet masses
We simulated the following mass ratios:
m_{ratio}= [3·10^{-3}, 1·10^{-3}, 3·10^{-4}, 1·10^{-4}, 3·10^{-5}, 1·10^{-5}]
corresponding to:
m_{planet}=[3 M_{jup}, M_{jup}, M_{sat}, 33 M_{earth}, 10 M_{earth}, 3 M_{earth}].

Radius and period
The semimajor axis (=radii) were logarithmically spaced from 0.01 to 63.1 AU:
s_{planet}=[0.01, 0.016, 0.025, 0.034, 0.063, 0.1, 0.16, 0.25, 0.40, 0.63, 1.0, 1.58, 2.51, 3.98, 6.31, 10.0, 15.8, 25.1, 39.8, 63.1]
corresponding to the periods [year]:
P= [0.0010, 0.0020, 0.0040, 0.0080, 0.016, 0.032, 0.063, 0.126, 0.25, 0.50, 1.00, 1.99, 3.98, 7.94, 15.9, 31.6, 62.8, 126, 251, 501].

Distance and apparent G-band magnitude
The distances were logarithmically spaced, for the most massive planets from 16.0 to 873 pc:
d=[16.0, 19.7, 24.4, 30.1, 37.1, 45.8, 56.6, 69.8, 86.2, 106.0, 131.0, 162.0, 200.0, 247.0, 305.0, 376.0, 464.0, 573.0, 707.0, 873.0]
which corresponds to an observed Gaia-band magnitude of:
G_{mag}=[5.70, 6.16, 6.62, 7.08, 7.53, 7.99, 8.45, 8.90, 9.36, 9.81, 10.27, 10.73, 11.19, 11.65, 12.11, 12.56, 13.02, 13.48, 13.93, 14.39]

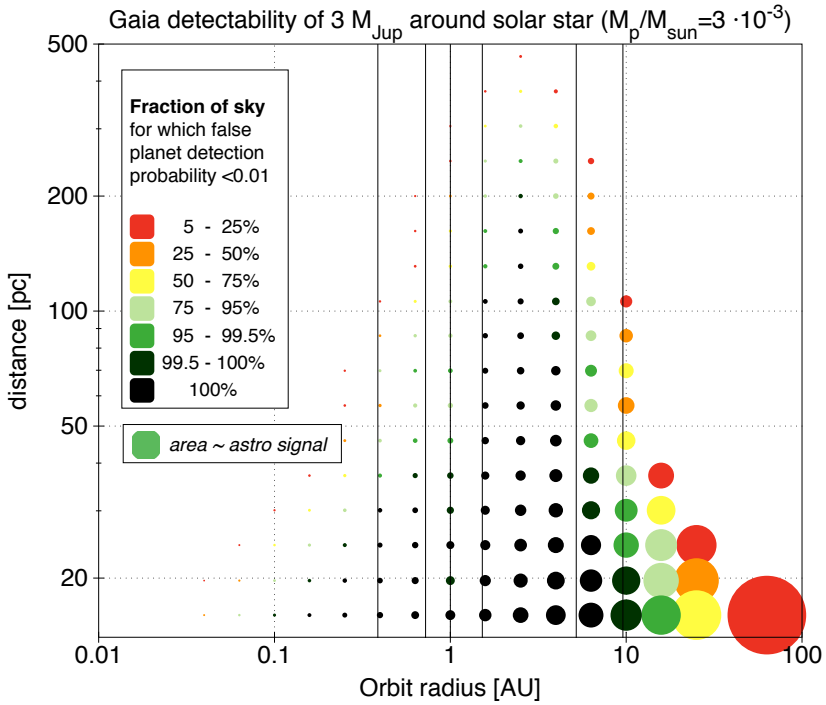

FIGURE 9: Figure demonstrating that the astrometric signal (indicated by the area of the circles) increases as function of semimajor axis and decreases as function of distance (conform Eq. (3)). It also shows that a larger astrometric signal does not necessarily mean a better detectability.

7.2 Degeneracy between parallax and one-year period

One of the orbital radii of the previous results was exactly aligned with 1 AU and it seemed to show a dip in detectability. This could suggest some degeneracy between parallax and a one-year period of an exoplanet. Therefore we made a second run in which we zoomed in around the one-year period and possible fractions of it, to see how significant the effect is. The result is given in Fig. 10, which clearly shows a dip around 1 yr (and possibly 0.5 yr). (The plots contain data for $\sim$ 1000 cases, or 1,000,000 simulated source detectabilities.)

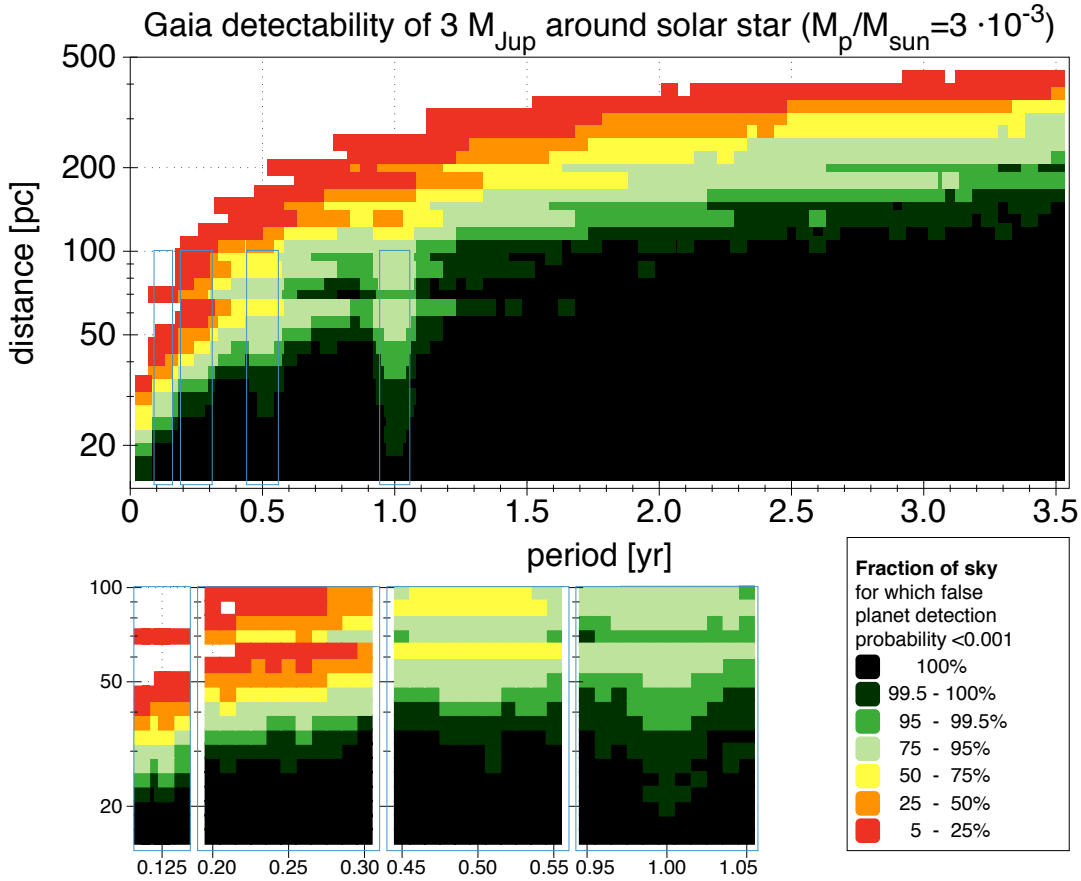

FIGURE 10: Examination plot that reveals a possible degeneracy between parallax and orbital period of one year and possible other fractions of one year. Zooms of four areas are shown on the bottom left, centred on 0.125, 0.25, 0.5 and 1.0 year.

8 Conclusions and discussion

In this report we have studied the detectability of a planet in circular orbit around a solar-type star.

Detectability shape in radius versus distance plot
For the most massive planet we examined, $3M_{jup}$, we find it to be detectable when it has a period between 4 months and 10 yr (outer bounds), with the detectability peaking around 5 yr. The detectability plots for all other planet masses follow *roughly* the same shape, peaking at the same place, only being shifted to a smaller distance. This can be understood as the astrometric signal scales linearly with the mass ratio m_{ratio} (Eq. 3), although it does not result in a *true* linear translation in distance because the accuracy of the observations is not the same for a system at different distances (i.e. different apparent magnitudes), as shown in Fig. 7.

Increased detectability for <5 yr period
The increase in detectability up till 5 yr seems also due to the increasing astrometric signal, which is linear dependence on semi-major axis s_{planet}.

Reduced detectability for >5 yr period
The turnover in detectability for period longer than 5 yr is likely to be due to an increasing degeneracy between planetary signal and proper motion. This can be understood by considering that the mission time was set to 5 yr and looking at Fig. 2: the signal that is being fitted by the 5 stellar astrometric parameters is that of the left panel (for Gaia 5 yr instead of 3 yr). If you consider now a planetary signal with a period of say 10 years, its isolated motion during 5 yr is that of half an ellipse (as the inclination is typically non-zero). Because this planetary motion is linearly added to the astrometric stellar signal we can just think of it as fitting the 5 stellar parameter model to this half ellipse, which obviously will absorb most of the half ellipse by a (linear) proper motion component, as this minimizes the χ^2. The longer the period with respect to the 5 yr mission, the smaller the fraction of the ellipse that is traced, and the better it is fitted with the proper motion.

Degeneracy between parallax and one-year period
Another degeneracy seems to be at work when we look at Fig. 10: the sudden loss of detectability when a planet has a one-year period. This is probably due to a partial degeneracy between parallax and planet signal. In general both trace an ellipse on the sky, alhough their ellipticity, phase and/or orientation is independent. It seems however likely that for one-year planet orbits at least a fraction of that orbital signal is absorbed in the parallax, depending on how well they are relatively aligned.
Note that this a realistic danger for Gaia: if as star has a planet with a period of one-year period that happens to be reasonably well aligned with the parallax motion, the planet could possible not be detected, and worse: the parallax estimate of the star would be biassed!

Gating signature
The last thing we would like to point out is that the 'gating' activity is visible in the detectability plots. For example in Fig. 10 we can clearly see a horizontal lines at distances of 70pc, which corresponds to G-mag 8.90, which is just beyond the gate at 8.84 (see Fig. 7) at which there is the largest jump that increases the accuracy (meaning that the noise in the observations suddenly goes down). This is in line with what we see in the vertical direction in Fig. 10 (this is quite clearly visible around a period of 0.7 year, where the detectability suddenly jumps up again at 70pc).

Final remarks
This project was more than great to do and it made me really excited about this subject. There are many things I could only mention here but not work out or quantify further due to lack of time. If possible, I would at some point come back to this subject and dive into it more deeply, because there are so many things that could be done with this kind of data! At least I tried to get as much out of it in the limited time available and I hope you enjoyed reading about it.

Acknowledgements: I would like to thank Anders Johansen for allowing me to choose my own project as part of his Planet Formation course. I would also like to thank Lennart Lindegren for his always valuable feedback on some of the statistical elements in this project.

9 References

Casertano, S., Lattanzi, M.G., Perryman, M.A.C., Spagna, A., 1996, apss, 241, 89, ADS Link

Casertano, S., Lattanzi, M.G., Sozzetti, A., et al., 2008, A&A, 482, 699, ADS Link

[SAG-AC-001], Colorado-McEvoy, A., 1999, *How many planets will Gaia detect?*, SAG-AC-001, URL http://www.rssd.esa.int/llink/livelink/open/357768

de Pater, I., Lissauer, J.J., 2010, *Planetary Sciences, 2nd edition*

[BH-002], Holl, B., Lindegren, L., Hobbs, D., 2009, *AGISLab - A facility for experimental astrometric solutions*, GAIA-C3-TN-LU-BH-002, URL http://www.rssd.esa.int/llink/livelink/open/2958464

Perryman, M., Hainaut, O., Dravins, D., et al., 2005, ArXiv Astrophysics e-prints, ADS Link

Perryman, M.A.C., 2000, Reports on Progress in Physics, 63, 1209, ADS Link

Sozzetti, A., 2005, pasp, 117, 1021, ADS Link

Wall, J.V., Jenkins, C.R., 2003, *Practical Statistics for Astronomers*

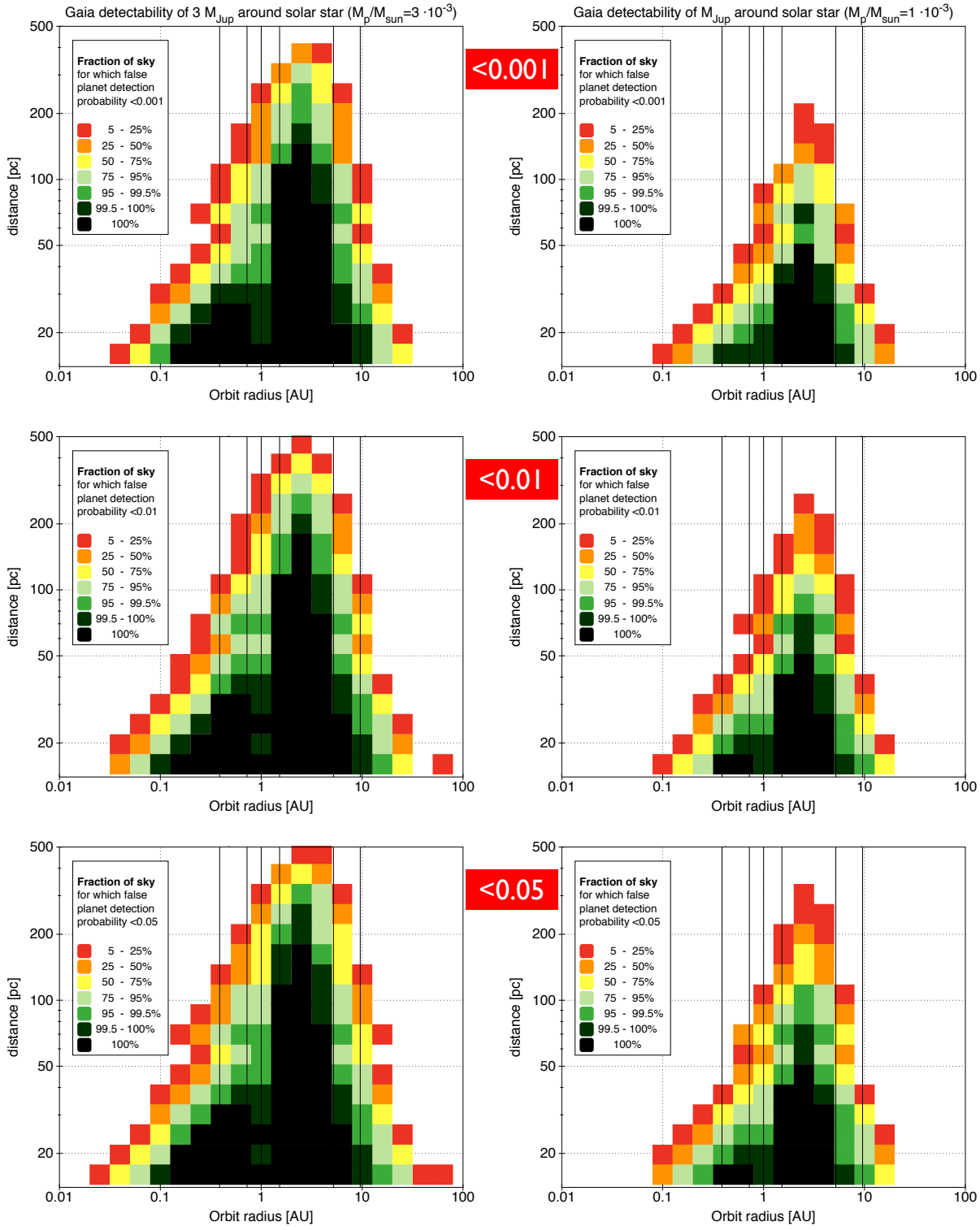

FIGURE 11: Detectability plots for $3M_{Jup}$ and M_{Jup}. Vertical black lines indicate the semi-major axis of the solar-system planets Mercury till Saturn.

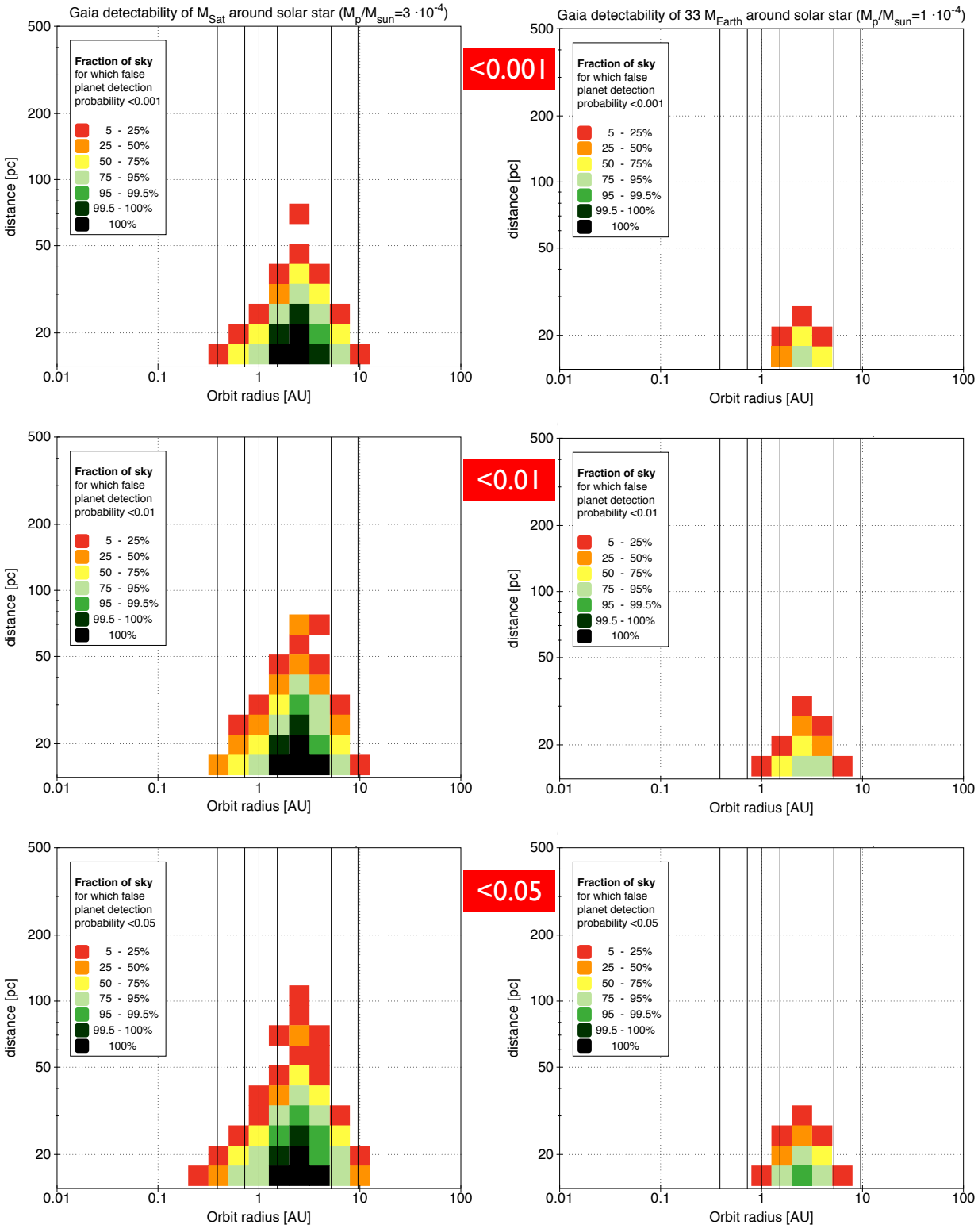

FIGURE 12: Detectability plots for M_{Sat} and 33 M_{Earth} (= 1/3 M_{Sat}). Vertical black lines indicate the semimajor axis of the solar-system planets Mercury till Saturn.

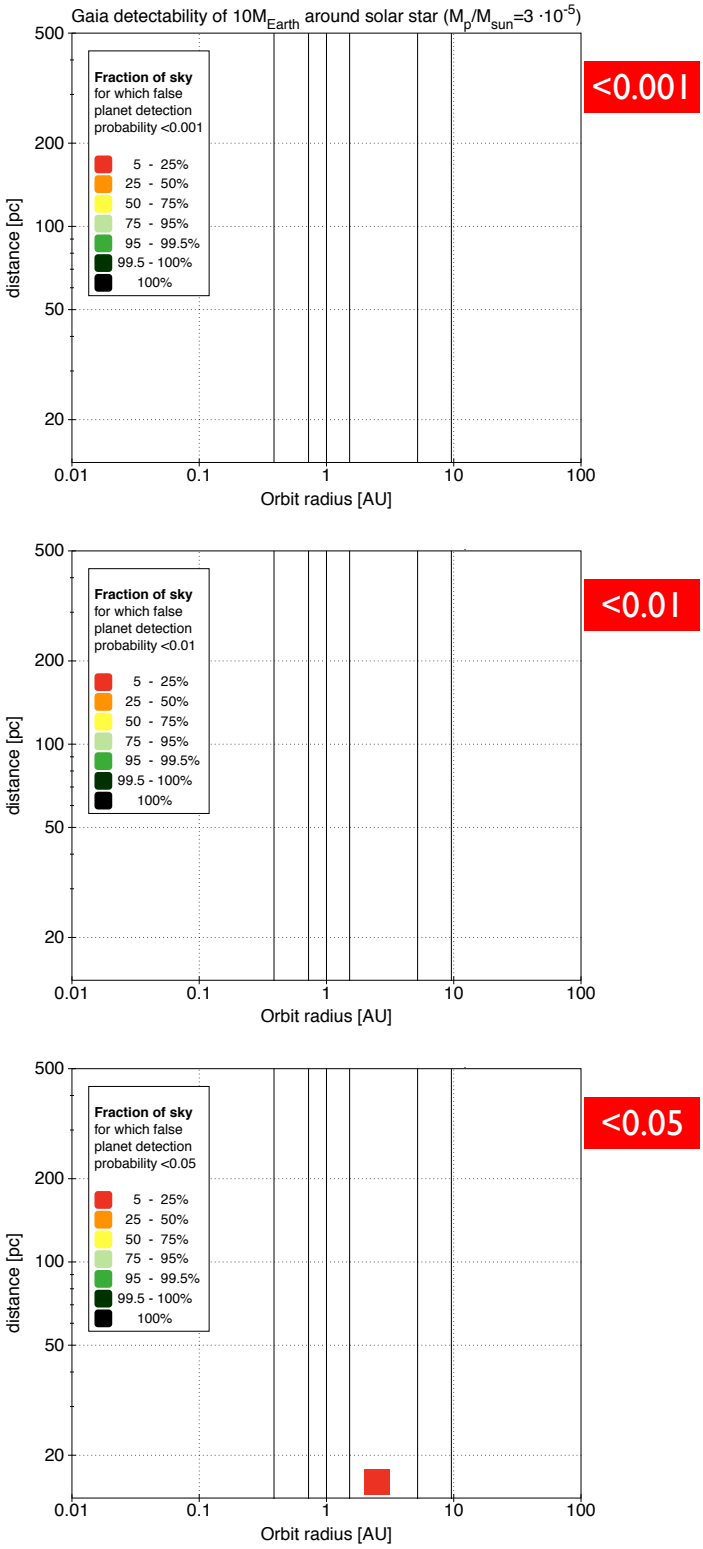

FIGURE 13: Detectability plots for 10 M_{Earth}. The plots for 3 M_{Earth} are omitted as they are completely empty. Vertical black lines indicate the semimajor axis of the solar-system planets Mercury till Saturn.